Eur. Phys. J. B **61**, 111–120 (2008)
DOI: 10.1140/epjb/e2008-00039-7

THE EUROPEAN PHYSICAL JOURNAL B

Phase diagram of the 3D bimodal random-field Ising model

N.G. Fytas[a] and A. Malakis[b]

Department of Physics, Section of Solid State Physics, University of Athens, Panepistimiopolis, 15784 Zografos, Athens, Greece

Received 23 October 2007
Published online 31 January 2008 –

Abstract. The one-parametric Wang-Landau (WL) method is implemented together with an extrapolation scheme to yield approximations of the two-dimensional (exchange-energy, field-energy) density of states (DOS) of the 3D bimodal random-field Ising model (RFIM). The present approach generalizes our earlier WL implementations, by handling the final stage of the WL process as an entropic sampling scheme, appropriate for the recording of the required two-parametric histograms. We test the accuracy of the proposed extrapolation scheme and then apply it to study the size-shift behavior of the phase diagram of the 3D bimodal RFIM. We present a finite-size converging approach and a well-behaved sequence of estimates for the critical disorder strength. Their asymptotic shift-behavior yields the critical disorder strength and the associated correlation length's exponent, in agreement with previous estimates from ground-state studies of the model.

PACS. 05.50+q – 64.60.Fr Equilibrium properties near critical points, critical exponents – 75.10.Nr Spin-glass and other random models

1 Introduction

The RFIM [1–15] has been extensively studied both because of its interest as a simple frustrated system and because of its relevance to experiments [16–21]. The Hamiltonian describing the model is

$$\mathcal{H} = -J \sum_{<i,j>} S_i S_j - h \sum_i h_i S_i, \qquad (1)$$

where S_i are Ising spins, $J > 0$ is the nearest-neighbors ferromagnetic interaction, and h_i are independent quenched random-fields (RF's) obtained here from a bimodal distribution of the form

$$P(h_i) = \frac{1}{2}[\delta(h_i - 1) + \delta(h_i + 1)]. \qquad (2)$$

h is the disorder strength, also called randomness, of the system. Various RF probability distributions, such as the Gaussian, the wide bimodal distribution (with a Gaussian width), and the above bimodal distribution (Eq. (2)) have been considered [22–33]. As it is well known, the existence of an ordered ferromagnetic phase for the RFIM, at low-temperature and weak-disorder, follows from the seminal discussion of Imry and Ma [1], when the space dimension is greater than two ($D > 2$). This has provided us with a general qualitative agreement on the sketch of the phase boundary separating the ordered ferromagnetic (**F**) phase from the high-temperature (strong-disorder) paramagnetic (**P**) phase. The phase boundary separates the two phases of the model and intersects the randomness axis at the critical value of the disorder strength, denoted hereafter as h_c. Such qualitative sketching has been commonly used in most papers for the RFIM [25,31,34–36] and close form quantitative expressions are also known from the early mean-field calculations [37]. However, it is generally true that the quantitative aspects of phase diagrams produced by mean-field treatments are very poor approximations. This applies also for the bimodal RFIM, for which, with the exception of the estimation of h_c from ground-state calculations [28–30], a reliable approximation of the phase diagram is still lacking. Furthermore, despite the 30 years of theoretical and experimental study the nature and scaling features of the transition of the RFIM are not yet well understood [38–40]. Nowadays, it is generally believed that the transition from the ordered to the disordered phase is continuous, governed by the zero-temperature random fixed-point [7,9,11], but a complete set of values of the critical exponents fulfilling scaling relations has not been established, despite the fact that several bounds [41] and further inequalities [8,42] for the critical exponents have been proposed, together with modified scaling relations [43]. It is also now quite clear that, the finite-size behavior of the system is obscured by

[a] e-mail: nfytas@phys.uoa.gr
[b] e-mail: amalakis@phys.uoa.gr

strong and complex finite-size effects, involving the violation of self-averaging [36,44–50]. In particular the issue of the order of the transition (first-order or continuous) has regained much interest after the recent observations of first-order-like features at the strong-disorder regime for both the bimodal [51] and the Gaussian RF distributions [52,53].

This work presents a careful and systematic numerical approach to the phase boundary of the bimodal RFIM in the low-temperature regime. The numerical approach, presented below, is a proposal that may be also useful to the study of other systems with complex energy landscapes, such as general random systems, spin glasses, proteins, and others. From our simulations, corresponding to systems with linear sizes L in the range $L = 4$–32, we perform a finite-size scaling analysis leading also to a refined value of the critical disorder strength h_c, in good agreement with the estimates obtained via the above mentioned ground-state techniques. We implement a novel approach that is based on the idea of entropic sampling in restricted energy spaces [54,55] together with a reliable extrapolation scheme and we produce accurate numerical data at the strong-disorder regime. Our analysis of the low-temperature part of the phase diagram provides us with a qualitative and also quantitative description of the phase diagram of the model, also at low values of the disorder strength, and produces good estimates for the critical disorder strength and the correlation length's exponent, in very good agreement with those from previous zero-temperature studies of the model.

The rest of the paper is laid out as follows. In the next Section we describe the numerical route implemented. In Section 3 we present in detail the low-temperature aspects of the phase diagram of the model. Finally, we summarize our conclusions in Section 4.

2 Numerical approach

There exist two distinct kinds of purely numerical approaches to the RFIM. The first approach utilizes Monte Carlo methods, including predominantly sophisticated simulation techniques, such as cluster algorithms and flat-histogram approaches, to study finite-temperature properties of the system [22,31,34,43,51,56–60], while the second approach utilizes graph theoretical algorithms to determine the ground-states and estimate the zero-temperature behavior of the RFIM [13,27–30,32,33,52,53,61]. This second approach, is grounded on the belief that the critical behavior of the model is governed by the non trivial RF fixed-point at zero-temperature [7,9,11].

In this work, we follow a novel numerical approach by combining current advances in simulation techniques. The proposed approach is well adapted and efficient for the study of the RFIM at the strong-disorder regime. Our scheme will be outlined and tested in this section for the 3D bimodal RFIM and it is hoped that it will provide a convenient and fast simulation tool for studying other similar disordered or complex systems. In effect, we shall use our earlier idea of the entropic implementation of the WL algorithm [55], to produce a faithful approximation of the exchange-field two-parametric DOS of the RFIM in an appropriate neighborhood of the disorder strength.

The WL algorithm [62] is one of the most refreshing improvements in Monte Carlo simulation schemes and has been already applied to a broad spectrum of interesting problems in statistical mechanics and biophysics [63]. Several implementations of the WL sampling technique have been carried out by many authors [51–53,63–73] and the present approach may be also seen also as a further contribution to the growing number of different applications of the WL method in the study of complex systems with rough energy landscapes. The original WL method has been already applied to the RFIM in previous studies concerning the properties of the system at specified values of the disorder strength. Such recent investigations have been presented for the bimodal [51] and also for the Gaussian RFIM [52,53], respectively. The present approach follows the implementation of the WL random walk used already in our recent studies of the RFIM [36,48,49]. In these studies we have carried out the WL random walk in a restrictive and more efficient fashion. This restrictive version, utilizes the so called critical minimum energy subspace (CrMES) technique [54,55] to locate and study finite-size anomalies of systems by carrying out the random walk only in the dominant energy subspaces. Generally, our finite-size scaling studies have shown that this restrictive practice can be followed in systems undergoing second-order [54,55,69–71] and also first-order transitions [72,73]. Details and tests of this approach for the 3D bimodal RFIM can been found in reference [48], where the thermal properties of the system at the disorder strength value $h = 2$ were studied.

In a subsequent paper [49] the magnetic properties of the RFIM were also considered by using the same restrictive scheme as an entropic sampling method. This simplification was introduced and tested for the first time in our earlier work [55] on the 2D and 3D Ising models and soon after that was used for the investigation and verification of some universal properties of the order-parameter distribution [69]. According to this we may estimate the magnetic properties of the systems by recording the two-parameter energy-magnetization (E, M) histograms in the final stage (high-levels) of the WL diffusion process. At the end of the process the final accurate WL (one-parametric) DOS $G(E)$ and the cumulative $H(E, M)$ histograms, are used to determine the magnetic properties of the system, by forming appropriate microcanonical averages of the order-parameter moments [49,55,69,71–73].

The above description may be seen as a convenient way to bypass the requirement of a two-parametric WL sampling process and a very similar approach will be implemented in this paper. We will now be recording, again in the high-levels of the WL diffusion process, the cumulative (exchange-energy, field-energy) two-parametric histograms, in order to produce an approximation for the two-parametric DOS of the RFIM. At this point, we should stress that any multi-parametric WL process is inevitably restricted to rather small lattices [62,74–77].

In fact the applications of such multi-parametric methods are substantially limited, since besides the immense time and excessive memory requirements, they very often face severe ergodic and/or convergence problems, depending on both the physical system and the algorithmic implementation. However, notable examples of such two-parametric studies, mainly on 2D systems, discussing also some of the above problems, have been carried out in the last 10 years. The most recent two-parametric investigation performed by Tsai et al. [77] concerns the critical endpoint of the 2D asymmetric Ising model with two and three-body interactions on the triangular lattice. This last study required several days of computer time and a quite large computer memory for the larger lattice size studied, consisting of $N = 42 \times 42$ lattice points. To our knowledge, this is also the largest system that has been reported by the two-parametric WL algorithm. Certainly, a similar two-parametric study is possible, although lacking, for the RFIM. However, the correspondingly large 3D system will have linear sizes of the order of $L = 12$, and this will be very small for our purposes. It will be seen in the next Section, that such lattice sizes are rather small for an accurate estimation of h_c of the bimodal RFIM.

We now proceed to give the details of the present entropic implementation of the WL approach. Carrying out the WL process at a particular value h of the disorder strength, we attempt to generate good approximations of the (exchange-energy, field-energy) two-parametric DOS for the RFIM in a neighborhood of h. An analogous approach was undertaken several years ago, before the invent of the WL method, by Deserno [78], who used flat-histogram techniques and also a restricted energy sampling to locate and study some properties of the tricritical point of the Blume-Capel model [79] on a simple cubic lattice. The extrapolation scheme described below subjects to the following WL process: depending on the lattice size, we use a total of at least $j_{WL} = 20$ WL iterations, producing at each iteration level well-saturated energy-histogram fluctuations [80] and obeying at least the 5% flatness criterion [54,55]. The reduction of the WL modification factor follows the usual rule: $f_{j+1} = \sqrt{f_j}$, $f_1 = e$ [54,55,62], and the range $j_{WL} \geq 16$ of the WL process is used for the recording and accumulation of the appropriate energy histograms (see definitions below).

To introduce our notation, let us now conveniently separate the Hamiltonian of equation (1) of the RFIM as follows

$$\mathcal{H}(x) = -J\mathcal{H}_J(x) - h\mathcal{H}_h(x) = -\mathcal{H}_J(x) - h\mathcal{H}_h(x), \quad (3)$$

where x denotes a spin state in phase space and we have set $J = 1$, since the behavior of the model depends only on the ration h/J. Assuming that the two-dimensional DOS $G(E_J, E_h)$ in the exchange and field variables $E_J = \mathcal{H}_J(x)$ and $E_h = \mathcal{H}_h(x)$ is known, the DOS with respect to the total energy $E = \mathcal{H}(x) = -E_J - h'E_h$ corresponding to any value h' of the disorder strength, can be deduced by summing over all pairs giving the particular value of the total energy

$$G_{h'}(E) = \sum_{E_J + h'E_h = E} G(E_J, E_h). \quad (4)$$

Let us further assume an entropic Markov process in which M spin states are selected from the phase space with probability $w_h(x)$ depending on the DOS $G_h(E)$, where E is the total energy of the spin state at the value h of the disorder,

$$w_h(x) \propto [G_h(E)]^{-1}. \quad (5)$$

Then, an approximation of the two-parametric (exchange-energy, field-energy) DOS of the RFIM in a neighborhood of h is provided by the expectation of the observable $\delta_{E_J;\mathcal{H}_J}\delta_{E_h;\mathcal{H}_h}$

$$\tilde{G}^{(h)}(E_J, E_h) \simeq \frac{1}{M w_h(x)} \sum_{x \in \{x\}_M} \delta_{E_J;\mathcal{H}_J}\delta_{E_h;\mathcal{H}_h} \simeq G_h(E)\frac{H^{(h)}(E_J, E_h)}{H^{(h)}(E)}, \quad (6)$$

where the last equality follows from equation (4), using the above approximate two-dimensional DOS in place of the exact and observing that $H^{(h)}(E) = \sum_{E_J + hE_h = E} H^{(h)}(E_J, E_h)$ and the double histogram $H^{(h)}(E_J, E_h)$ is the above sum of the observable $\delta_{E_J;\mathcal{H}_J}\delta_{E_h;\mathcal{H}_h}$. The superscript (h) in the quantities in the above equation is only a reminder of the fact that the simulation is performed at the disorder strength value h. It should be noted that this notation does not mean an h-dependence, but rather a statistical indirect influence on the reliability of the histogram recordings and accordingly on the two-dimensional DOS. In our approach the ratio of histograms in the above equation (6), by the assumed Markov process, is replaced by the ratio developed during the final high-levels ($j_{WL} \geq 16$) of the WL process. Denoting these latter histograms by $H^{(h)}_{WL}(E_J, E_h)$ and $H^{(h)}_{WL}(E)$ and by $\tilde{G}_h(E)$ the WL DOS, as modified at the final level of the process, our final approximation reads

$$\tilde{G}_{WL}(E_J, E_h) \simeq \tilde{G}_h(E)\frac{H^{(h)}_{WL}(E_J, E_h)}{H^{(h)}_{WL}(E)}. \quad (7)$$

The above approximation provides in conjunction with the skew summing procedure of equation (4) a suitable extrapolation scheme which can be used for the study of the RFIM in the neighborhood of the disorder value h, used for the WL simulation. This extrapolation program will be applied in the next Section for the study of the finite-size development of the phase diagram of the bimodal RFIM at the strong-disorder regime. From our previous studies it has been verified [55,69] that the detailed balance condition is quite well satisfied at the high-levels of the WL process and the recording of appropriate histograms produces faithful and good approximations. Therefore, it is hoped that the proposed extrapolation program will not

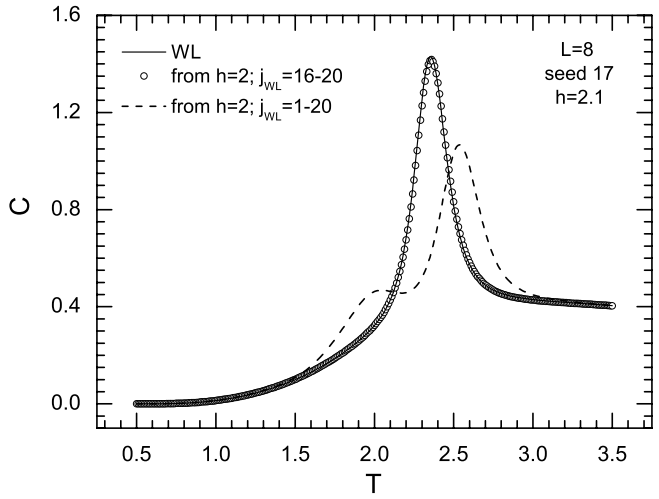

Fig. 1. Illustration of the effect of the violation of the detailed balance in the early WL iteration levels. Details of the shown approximations are also given in the text.

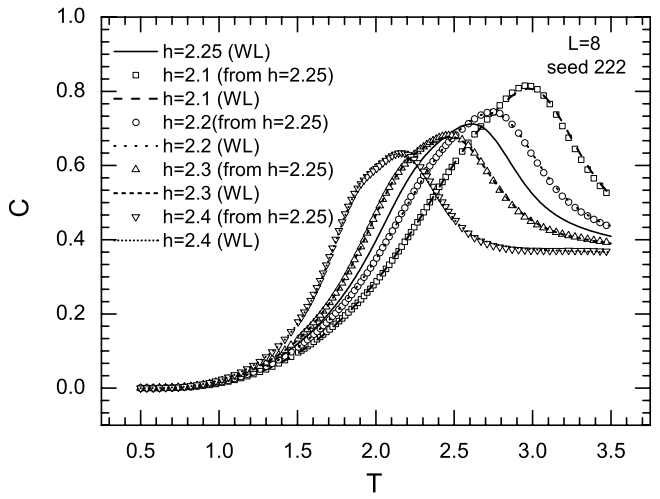

Fig. 2. Specific heat curves for a certain RF of the lattice size $L = 8$. Illustration of the behavior for several values of the disorder strength obtained by direct WL simulation (lines) and by the extrapolation scheme (points).

produce systematic errors, besides the expected statistical fluctuations. However, for safety reasons, we shall use relatively small values for the extrapolation shift parameter $|h - h'|$, at most of the order of 7% of the disorder strength value, and a rather loose restriction of the energy space in which the main WL simulation is performed. In particular, in most of our simulations performed at $h = 2.25$ the energy spectrum for the simulation was restricted only from the high-energy side, while the entire low-energy part of the spectrum down to the ground-state was included (see also the discussion below). For the restriction of the high-energy side we used our data from our previous study of the model at the value $h = 2$. In this way the WL sampling extends to all energy values with a significant contribution to the finite-size anomalies of the model for all values $h > 2$. For moderately large lattice sizes ($L > 12$), this practice is not the optimum choice. This is because, besides the energy states contributing to the range $h = 2.1$–2.4, used in our extrapolation program, one simulates also the part of the energy spectrum in the neighborhood of the ground-states in which the convergence of the algorithm is very slow. Thus, for the larger lattice sizes, one may avoid this ground-state neighborhood, as we have done for the sizes $L = 26$ and $L = 32$.

Before moving to the presentation of our results, let us end this Section by presenting some tests on the reliability of the proposed approach. Figure 1 illustrates the accuracy of our practice of using the high-levels of the WL process as an entropic sampling method. The curves and points shown represent three different approximations of the specific heat for a particular RF on a lattice of linear size $L = 8$. The solid line is the directly simulated specific heat by the WL method at $h = 2.1$ and should be seen as an almost exact result. The open circle points represent an excellent approximation obtained for the value $h = 2.1$ by using a WL simulation at $h = 2$ and our extrapolation scheme, using the high-WL iteration levels ($j_{WL} = 16$–20) for the recording the double (exchange-energy, field-energy) histograms. Finally, the dashed line shows some quite dramatic distortion effects obtained by using the whole ($j_{WL} = 1$–20) WL iteration range for the recording of the above two-dimensional energy histograms. This is of course an example, showing possible subtle effects coming from a significant violation of the detailed balance condition in the early WL iteration levels.

A second test showing now the reliability of our extrapolation scheme is presented in Figure 2. Here we show specific heat curves, in the range $h = 2.1$–2.4, obtained by the proposed extrapolation scheme from a WL simulation performed at $h = 2.25$, together with the results obtained independently via direct WL simulation at the corresponding disorder strength values. For values very close to $h = 2.25$, the two different approximations coincide, and even for the values $h = 2.1$ and $h = 2.4$ there are only very small deviations, mainly around the peaks. The locations of the pseudocritical temperatures are very weakly dependent on the extrapolation scheme and are therefore quite accurately determined by the method. The effects on ensemble averages will be expected to be even weaker. This is illustrated in our final test concerning the pseudocritical temperatures obtained from the ensemble average specific heat curve, used in the next Section for the description of the phase diagram. The average specific heat is defined as usually [58,59]

$$[C]_{av} = \frac{1}{Q} \sum_{q=1}^{Q} C_q(T), \tag{8}$$

where the index $q = 1, \ldots, Q$ runs over the number of disorder realizations. Figure 3 concludes this Section by a comparison of two approximations of the average specific heat curve $[C]_{av}$ obtained from an ensemble of $Q = 35$ realizations and corresponding to the disorder strength value $h = 2.2$. The solid line is the average curve obtained by a direct WL simulation at $h = 2.2$, while the

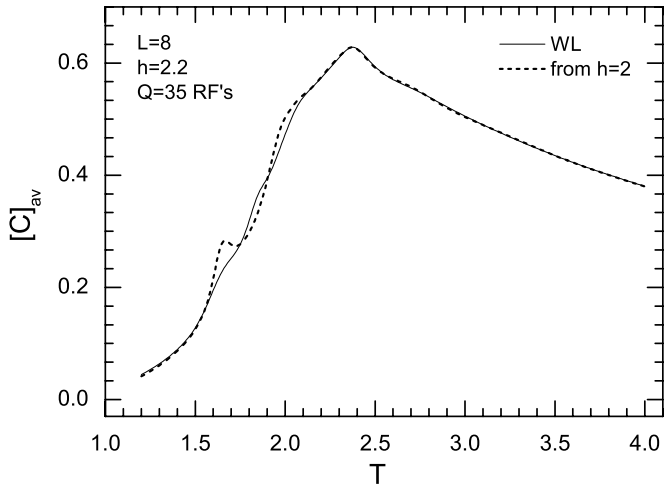

Fig. 3. Average specific heat curve at $h = 2.2$, obtained by direct WL simulation (solid line) and by extrapolation (dotted line), for lattice size $L = 8$ averaged over $Q = 35$ RF's.

dashed line represents the approximation of the extrapolation scheme based on a WL simulation on the same ensemble at the value $h = 2$. Clearly, the locations of the two pseudocritical temperatures coincide and the two specific heat peaks are in excellent agreement.

3 Phase diagram

We aim here to present a reliable approximation of the phase diagram of the 3D bimodal RFIM at the strong-disorder regime and provide an accurate estimate for h_c (independent from the ground-state approach). Despite the general qualitative agreement between different approaches on the phase diagram of the model, the various estimations throughout the literature vary in a rather wide range. This diversity on the numerical estimation of the phase diagram is true for both the Gaussian and the bimodal distributions and is generally reflected in the wide range of estimates for h_c. Thus, for the Gaussian RFIM the values for h_c span the range $h_c = 2.26$–2.37, despite the fact that these values are mainly estimated via the same ground-state approach [13,27,28,30,32–34,43,53,61]. On the other hand, there are fewer attempts devoted to the estimation of the phase diagram of the bimodal RFIM and the corresponding estimates for h_c, obtained again via the ground-state approach, are restricted in a smaller range, i.e. $h_c = 2.20$–2.25 [27,28,30]. Our previous attempt to estimate the phase diagram using a high-temperature (weak-disorder: $h = 0.5$–2) numerical study yielded an overestimation for h_c, namely $h_c = 2.42(18)$ [36]. However, we will show here, that an accurate estimation of the phase diagram is possible by a more systematic low-temperature (strong-disorder: $h \geq 2$) numerical study. In this case, we will find a much lower estimate for h_c that agrees favorably with the estimates given above from the ground-state approach. Additional good comparisons with some phase diagram points, estimated earlier in the literature, provide evidence that our final proposal for the phase diagram may be a reliable and competent approximation for the whole disorder strength range.

We proceed here to analyze our numerical data at the strong-disorder regime. Using our entropic implementation of the WL method and the extrapolation procedure, outlined in the previous section, we have generated numerical data for the following lattice sizes: $L \in \{4, 8, 12, 16, 20, 26, 32\}$. For lattice sizes in the range $L = 4$–20 we have simulated 20 RF's, whereas for the larger sizes $L = 26$ and $L = 32$, 10 realizations of the RF have been simulated. For each lattice size and each realization, we performed a WL simulation in an appropriate energy subspace, restricted only from the high-energy end and including the entire low-energy spectrum down to the ground-state, with the exception of the sizes $L = 26$ and $L = 32$ for which the very close to the ground-sate energy levels were avoided. The WL simulation was performed at the disorder strength value $h = 2.25$ and the accumulated double (exchange-energy, field-energy) histogram was then used to approximate the two-parametric DOS (Eq. (7)) and finally, the DOS $G_{h'}(E)$ (Eq. (4)) and the thermal properties of the system for various values of randomness in a neighborhood of the simulated value $h = 2.25$. In order to construct the average specific heat curve (Fig. 3) and to identify via its peak a pseudocritical temperature $T_{L;h}$, representing the ensemble of RF's at the particular lattice size, a summation over the realizations was performed, as in equation (8). As discussed earlier and illustrated in Figures 1–3, the described extrapolation scheme provides a reliable approximation of the location of the maximum of the average specific heat curve. The systematic shift of the individual specific heat peaks, shown in Figure 2, for higher values of h, will be reflected in the corresponding shifts of the peaks of the average specific heat curves, as should be expected, providing us the necessary information for the finite-size analysis. The locations of all these specific heat peaks, for all lattice sizes mentioned above, were calculated from our simulation data at $h = 2.25$, and their extrapolations to other neighbor h-values, for the following set I of disorder values, set I: $h' = \{2.1, 2.15, 2.2, 2.25, 2.3, 2.35, 2.4\}$. For the lattice size $L = 12$, an additional entropic WL sampling was carried out at $h = 2$, using now a larger ensemble of $Q = 250$ RF's. Again, using the extrapolation procedure of equations (7) and (4) the specific heat peaks corresponding to the following set II of disorder values were located, set II: $h' = \{1.7, 1.8, 1.9, 2, 2.1, 2.2\}$.

Let us attempt now a finite-size analysis using the size-shifts of the pseudocritical temperatures of the averaged specific heat curves for some particular value of the disorder. The inset of Figure 4 illustrates fitting attempts of these size-shifts for three values of the disorder. The range $L = 8$–32 is used in these fits by assuming the usual power law:

$$T_{L;h} = T_{c;h} + a_h L^{-1/\nu_h}. \tag{9}$$

The critical temperatures $T_{c;h}$, resulting as limiting values of the corresponding pseudocritical temperatures, for the attempts shown in the inset of Figure 4, are 1.297(237),

0.894(264), and 0.659(299), for the disorder strengths $h = 2.1$, 2.15, and 2.2 respectively. We have excluded, from our fitting attempts here, the lattice size $L = 4$ in order to eliminate the influence from the very small L-behavior and this practice will be followed and further discussed in the sequel. Following the same fitting procedure, again in the range $L = 8$–32, for $h = 2.25$ we find that the corresponding critical temperature becomes now negative, i.e. $T_{c;2.25} = -0.18$. This fact shows that, within our fitting scheme, the value of the disorder strength $h = 2.25$ is an upper bound for the critical disorder strength. Noteworthy, that if we use the range $L = 4$–32 instead, the negative sign for the critical temperature will appear at the value $h = 2.35$, which however appears to be a rather overestimating bound for the critical randomness. Thus, only the three points $h = 2.1$, $h = 2.15$, and $h = 2.2$ (filled circles) resulting from the fits shown in the inset of Figure 4 can be used to approximate the phase diagram. In order to find one more point of the phase diagram we shall now also use our earlier numerical data [48] (from rather large $Q = 500$–1000 ensembles of RF's) for the disorder strength $h = 2$. Using the above fitting practice in the range $L = 8$–32 we find from the general pseudocritical temperature shift behavior the limiting value $T_{c;2} = 1.848(188)$ (open triangle), which is just inside the estimate bounds given in our previous paper ($T_{c;2} = 2.03(18)$) using sizes in the range $L = 4$–32 [48].

The above four approximate phase diagram points, corresponding to the disorder strength values $h = 2$, 2.1, 2.15, and 2.2, will be now used to find a phenomenological representation of the phase diagram of the bimodal RFIM. Let us first attempt an elliptical fit using the following ansatz

$$h = h_c \sqrt{1 - \left(\frac{T_{c;h}}{\tau}\right)^x}. \qquad (10)$$

The rescaling temperature factor τ in equation (10) will be handled either as a free-parameter during the fit, or as a fixed-parameter using the best known estimate for the critical temperature of the zero-field Ising model, namely $T_{c;0} = 4.51153$ [81]. The resulting phase diagrams almost coincide (see Fig. 4 where for clarity reasons only the latter case is shown) and are described respectively by the following (h_c, τ, x; χ^2) parameter values, including the value of the χ^2-test: (2.212(29), 4.50394(778), 1.862(87); $\sim 10^{-4}$) and (2.215(35), 4.51153, 1.847(92); $\sim 10^{-4}$), respectively. Thus, our fitting attempts with equation (10) produce a value for the critical disorder which is very close to the estimates obtained from the zero-temperature studies of the model [27,28,30]. Furthermore, the fitting using the temperature rescaling factor τ in equation (10) as a free-parameter produces a fairly good estimate for the critical temperature of the zero-field Ising model [81].

As an alternative to the above elliptical fit, we have also considered for comparison the following power-law ansatz [36]

$$h = h_c \left(\frac{T_{c;0} - T_{c;h}}{T_{c;0}}\right)^x. \qquad (11)$$

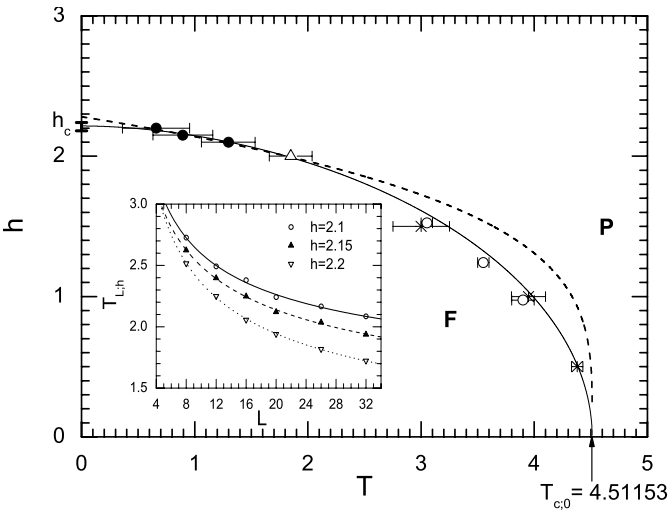

Fig. 4. Approximations of the phase diagram of the 3D bimodal RFIM. Two fitting attempts are shown. The solid line corresponds to the elliptical ansatz (10) giving $h_c = 2.215(35)$, while the dashed line to the power-law ansatz (11) giving $h_c = 2.277(49)$. The range of ground-state estimates for h_c and the zero-field's critical temperature $T_{c;0} = 4.51153$ are marked on the axis. The inset shows the shifting of the pseudocritical temperature $T_{L;h}$ for three values of the disorder strength, i.e. $h = 2.1$, 2.15, and 2.2.

The attempt to fit the same data to this law is illustrated also in Figure 4 by the dashed line. In this case we find a noticeable overestimation of h_c, namely $h_c = 2.277(49)$ and a much larger (by a factor of 70) value of χ^2 of the fit. Therefore, we conclude that the elliptical law of equation (10) provides a better representation of the phase diagram of the RFIM. Of course, our attempt above aims only at a numerical approximation for the main part of the diagram and not at the correct asymptotic behavior at its ends. For instance, the behavior of the phase diagram at a very small neighborhood around the critical temperature of the pure system, is expected to be determined by the susceptibility exponent γ of the pure system [37,39,82], as follows from the phenomenological renormalization arguments of reference [39]. Accordingly, the slope of the phase diagram at this end is expected to behave as $\delta h \sim (\delta T)^\gamma$ (where $\gamma = 1.2358$ for the pure 3D Ising model [83]) and not with the exponent 1/2 of the ansatz (10). It appears that similar elliptical laws have been also used previously by other authors for the Gaussian RFIM [31,34], although these were not stated explicitly.

Finally, we would like to note that we have included in Figure 4 some more data points for smaller values of the disorder strength from previous numerical works. These are the data for $h = 0.5$, 1, and 1.5 (shown by stars in the figure) from our previous investigation of the phase diagram of the model [36] and three more points (open circles) estimated by Rieger and Young [58]. These points are close enough to our approximate phase diagram and the small deviation comes possibly from the fact that these have been estimated, in both cases, by applying

equation (9) to rather small sizes: $L \leq 24$ and $L \leq 16$, respectively (see also the discussion below).

At this point, let us comment on the significance of our notation concerning the shift exponent ν_h in equation (9). As mentioned earlier, we have tried to avoid the influence of the very small L-behavior in our estimates, thus excluding from our fitting attempts the data for $L = 4$. This is a compromise followed because in our study (and in effect in all finite-temperature studies) a rather restricted L-range is available for performing finite-size scaling analysis. However, it has been pointed out in reference [36] that the estimates based on such restricted ranges should not be completely trusted and this may be particularly true for the shift exponent ν_h. For instance, the range $L = 4$–24 will produce quite different estimates, for both $T_{c;h}$ and ν_h, from those obtained above from the range $L = 8$–32 and this fact, together with the use of the power-law in equation (11), are the two reasons behind our earlier overestimation of h_c ($h_c = 2.42(18)$ in Ref. [36]). The general asymptotic behavior of the RFIM follows different complex routes that appear to strongly depend on the value of the disorder strength h and different ranges of lattice sizes may be needed in order to approach the asymptotic behavior for different values of disorder strengths. Even the observation of an appreciable disorder strength dependence on ν_h, should be reluctantly identified as a possible violation of universality along the phase boundary, although this violation of universality is one of the strongly supported scenarios in the literature [29]. The violation of universality for the case of the 3D RFIM has been discussed a few years ago by Sourlas [29]. Equivalent studies of universality violations have been reported also in other glassy systems [84], reenforcing the view that the concept of universality in complex systems is not fully clarified.

We proceed now with an alternative estimation of the critical disorder strength. Firstly, let us point out that for each value of L, our data can be used to produce a finite-size phase diagram. Provided that the phase diagram points do not decline appreciably from the above elliptical law, we may attempt to construct a finite-size sequence of diagrams by using the finite-size version of equation (10)

$$h = h_{c;L}\sqrt{1 - \left(\frac{T_{L;h}}{\tau_L}\right)^x}, \qquad (12)$$

where now the rescaling temperature factor τ_L may be either handled as a free-parameter during the fit or as a fixed-parameter at the corresponding zero-field's Ising model pseudocritical temperatures taken from Table 4 of reference [54]. Using this latter choice for τ_L, Figure 5 provides a test of this approach producing two very similar phase diagrams for the size $L = 12$. The two diagrams are obtained using the two different sets of phase diagram points corresponding to set I and set II of the disorder strength values. The first set of points (filled triangles) is determined over an ensemble of $Q = 20$ realizations of the RF and corresponds to set I, i.e. simulation at $h = 2.25$ and suitable extrapolation in the range $h = 2.1$–2.4. The other set of points (open circles) is determined over a larger ensemble of $Q = 250$ realizations of the RF and corresponds to set II, i.e simulation at $h = 2$ and extrapolation in the range $h = 1.7$–2.2. The application of the elliptical law (12) gives the two very similar phase diagrams shown in Figure 5 by the solid and dashed lines for the two set of points, respectively. These two diagrams, with comparable values for χ^2 of the order of 10^{-7}, come together to the same point at $T = 0$, giving the value $h_{c;12} = 2.56$ for the finite-size ($L = 12$) critical disorder strength. For illustration reasons, we have also included in this figure the attempt using the corresponding finite-size version of equation (11) for the set of points obtained from the simulations at the value $h = 2.25$ (dotted line). Again the χ^2 quality of the fit is worst for the power-law ($\chi^2 = 10^{-5}$) and produces a clear overestimation for the pseudocritical disorder strength of the order of $h_{c;12} = 2.77(5)$. The comparison between the two finite-size elliptical phase diagrams, corresponding to the two sets of points ($h = 2.25$ and $h = 2$), is on the other hand very convincing. Thus, Figure 5 provides strong evidence in favor of our choice of using in our simulations for all lattice sizes the strong-disorder regime corresponding to the value $h = 2.25$. In particular it shows that our data based on only the $Q = 20$ RF's are sufficient for our proposes of estimating the phase diagram.

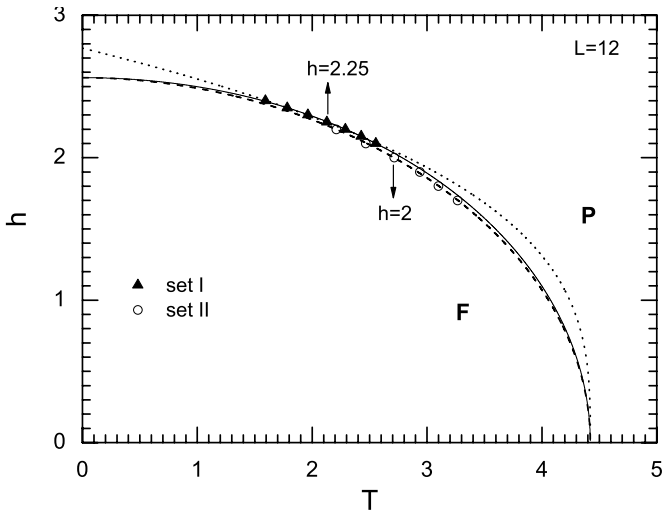

Fig. 5. Finite-size elliptical phase diagrams for $L = 12$ using two different extrapolation sets of disorder strength values (set I (filled triangles) and set II (open circles)) and different realizations ensembles. The solid and dashed lines are elliptical fits of the form (12) with comparable values of χ^2 of the order of 10^{-7} giving for the pseudocritical disorder strength the values $h_{c;12} = 2.56(3)$ and $h_{c;12} = 2.56(2)$, respectively. The application of the finite-size version of the power-law (11), shown by the dotted line, has a larger value of $\chi^2 = 10^{-5}$ and produces an overestimation for the pseudocritical disorder strength: $h_{c;12} = 2.77(5)$.

Figure 6 presents the finite-size elliptical phase diagrams for lattice sizes in the range $L = 8$–32, using set I of the disorder strength values. For the lattice size $L = 4$ we have not drawn a finite-size phase diagram, since it is

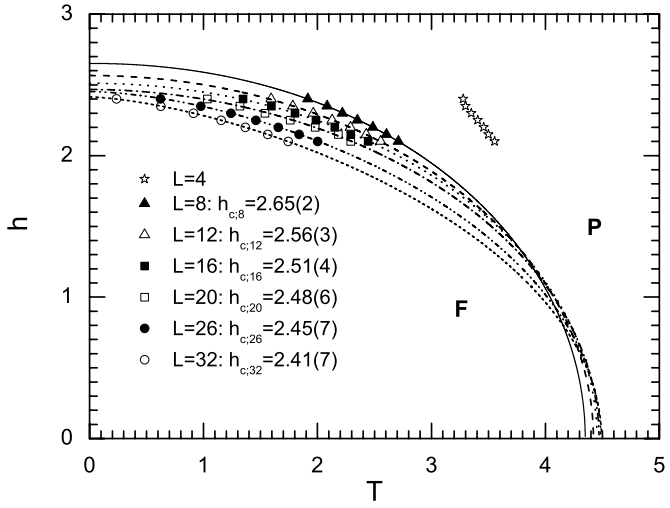

Fig. 6. Finite-size elliptical phase diagrams for lattice sizes in the range $L = 8$–32, using set I of the disorder strength values. The drawn lines represent the finite-size elliptical fittings according to equation (12), in which the rescaling temperature factor τ_L was fixed at the corresponding zero-field's Ising model pseudocritical temperatures.

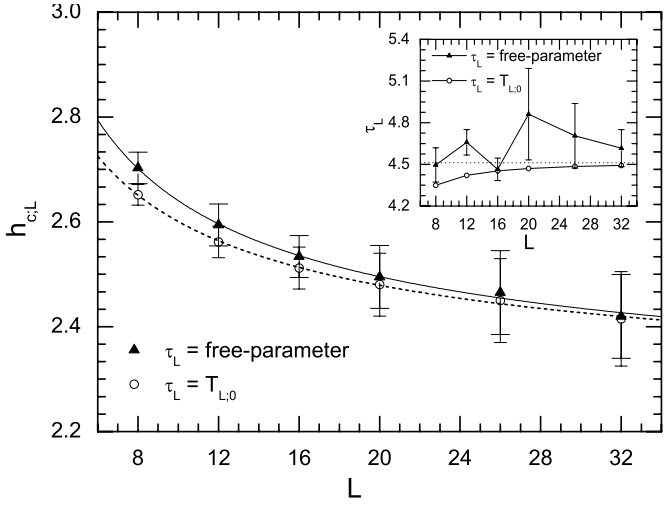

Fig. 7. Shift behavior of the finite-size critical disorder strengths $h_{c;L}$. The inset shows the oscillations in the values of τ_L, when this parameter is handled as a free-parameter. Their behavior follows the correct trend, approaching the zero-field's $T_{c;0} = 4.51153$ [81] (dotted line).

quite evident from the corresponding open star points in Figure 6 that they decline very early, at about the value $h = 2.2$, from the elliptical law. No such deviation is observed for the other lattice sizes, within the set I of disorder values, and this fortifies our choice to use the particular set I for these lattice sizes. Of course, an attempt to push our approach to even larger lattices may require a WL simulation at $h = 2.2$ and a corresponding set of somewhat smaller disorder values. The drawn lines in Figure 6 represent the finite-size elliptical fittings according to equation (12), in which the rescaling temperature factor τ_L was fixed at the corresponding zero-field's Ising model pseudocritical temperatures. For clarity the diagrams using τ_L as a free-parameter are not shown. However, the main frame and the inset of Figure 7 illustrate the smoothness of the both fitting schemes and reveal a convincing and regular shift-behavior of the finite-size critical disorder strengths $h_{c;L}$. This behavior allows now a finite-size analysis for the estimation of h_c. The solid and dashed lines show good quality fits to the following usual shift power-law

$$h_{c;L} = h_c + bL^{-1/\nu}. \tag{13}$$

Thus, the fitting attempts in Figure 7 produce estimates for the asymptotic value of the critical disorder strength h_c, and the corresponding shift-exponent ν. The fitting scheme based on the estimates of the pseudocritical disorder strengths $h_{c;L}$ (open circles in Fig. 7), produced by fixing the rescaling temperature factor τ_L at the corresponding zero-field's Ising model pseudocritical temperatures, i.e. $\tau_L = T_{L;0}$, gives $h_c = 2.219(83)$ and $\nu = 1.806(390)$. Finally, the fitting attempt based on the corresponding $h_{c;L}$ estimates (filled triangles in Fig. 7), produced by using τ_L as a free-parameter, results in a almost identical estimate for the critical disorder, i.e. $h_c = 2.219(65)$ but a slightly lower estimate for the shift-exponent $\nu = 1.640(423)$. From the inset of Figure 7 we may note some oscillations in the values of τ_L, when this is handled as a free-parameter, which however appear to follow the correct trend so that τ_L will approach $T_{c;0}$ (dotted line) with increasing lattice size. In both cases, the estimates for h_c compare very well with those obtained above from fitting equation (10) in Figure 4 and also with those of the ground-state approach [27,28,30]. Despite the deviation of the two estimates for the shift-exponent and the relatively very large variation of ν in the literature (for both the Gaussian and bimodal cases), it is of interest to compare here the estimate of the second case ($\nu = 1.64$) with the estimates 1.67(11) and 1.66(8) of references [28] and [30] respectively, obtained by zero-temperature simulations.

The above observations provide concrete evidence in favor of our present approach. It appears that, this method may be capable to produce, if further pushed to larger lattices, even more accurate estimates for both the critical disorder strength and also the $T = 0$ correlation length exponent, assuming that its behavior follows the observed shift-behavior of our finite-size projections $h_{c;L}$. It is well known from the general scaling theory that, even for simple models, the equality between the correlation length's exponent and the shift exponent is not a necessary consequence of scaling [85]. Of course, it is a general practice to assume that the correlation length behavior can be deduced by the shift behavior of appropriate thermodynamic functions. In our view, the recent strong version of the zero-temperature fixed-point scenario by Wu and Machta [52,53], supports the above assumption that the finite-size projections $h_{c;L}$ are appropriate shifting parameters. The thermal states of Wu and Machta (see Fig. 4 of

Ref. [52]) at temperatures close to the finite-size anomalies are strongly correlated to the ground-states at disorder strength values close to the zero-temperature critical point and this strong correlation may be seen as a phenomenological justification of our assumption.

4 Conclusions

A numerical approach combining well-known techniques has been proposed as a convenient alternative for the study of disordered systems. Within this approach, the well-known WL algorithm is used, at its final stage, as an entropic sampling method, and multi-parametric histograms, appropriate for the study of the system, are produced. The main advantage of this scheme is that the requirement of multi-parametric WL sampling is surpassed and by using the DOS, obtained via the WL method, and the accumulated histogram information, the thermal properties of the disordered system may be obtained in a neighborhood of the simulated disorder strength value. The numerical techniques presented in this paper may find further applications in the study of critical properties of other challenging disordered systems. Via the above approach, we have studied the general size-shift behavior of the low-temperature part of the phase diagram of the 3D bimodal RFIM. Our detailed analysis provided an overall reliable representation of the main part of the phase diagram, yielding accurate estimates for the critical disorder strength. These estimates are in agreement with those from previous zero-temperature studies of the model including the estimates for the correlation length's exponent.

As a closing remark, we would like to mention that, using our WL DOS's — for some typical RF realizations, at the simulated disorder strength value $h = 2.25$ – we have also observed, for the larger sizes studied, first-order-like double peaks in the energy probability densities, in agreement with the recent observations of Hernández and Ceva [51], and Wu and Machta [52,53], mentioned in the introduction. This main issue appears to be still a matter of controversy and we are currently carrying out further research in order to clarify the persistence (or not) of such first-order-like characteristics in the asymptotic limit. However, the full resolution of this aspect requires an understanding of the complex finite-size effects of the RFIM at the strong-disorder regime and substantial computer resources to be devoted for the simulation of large ensembles of RF realizations in a convenient neighborhood of disorder strength values.

The authors would like to thank Professor A.N. Berker for useful discussions. This research was supported by the Special Account for Research Grants of the University of Athens under Grant No. 70/4/4071. N.G. Fytas acknowledges financial support by the Alexander S. Onassis Public Benefit Foundation.

References

1. Y. Imry, S.-K. Ma, Phys. Rev. Lett. **35**, 1399 (1975)
2. A. Aharony, Y. Imry, S.-K. Ma, Phys. Rev. Lett. **37**, 1364 (1976)
3. A.P. Young, J. Phys. C **10**, L257 (1977)
4. G. Parisi, N. Sourlas, Phys. Rev. Lett. **43**, 744 (1979)
5. G. Grinstein, S.-K. Ma, Phys. Rev. Lett. **49**, 685 (1982); G. Grinstein, S.-K. Ma, Phys. Rev. B **28**, 2588 (1983)
6. J.Z. Imbrie, Phys. Rev. Lett. **53**, 1747 (1984)
7. J. Villain, Phys. Rev. Lett. **52**, 1543 (1984); J. Villain, J. Phys. (Paris) **46**, 1843 (1985)
8. M. Schwartz, Phys. Lett. **107A**, 199 (1985); M. Schwartz, J. Phys. C **18**, 135 (1985); M. Schwartz, A. Soffer, Phys. Rev. Lett. **55**, 2499 (1985); M. Schwartz, A. Soffer, Phys. Rev. B **33**, 2059 (1986)
9. A.J. Bray, M.A. Moore, J. Phys. C **18**, L927 (1985)
10. A. Houghton, A. Khurana, F.J. Seco, Phys. Rev. Lett. **55**, 856 (1985); A. Houghton, A. Khurana, F.J. Seco, Phys. Rev. B **34**, 1700 (1986)
11. D.S. Fisher, Phys. Rev. Lett. **56**, 416 (1986)
12. K. Binder, A.P. Young, Rev. Mod. Phys. **58**, 801 (1986)
13. A.T. Ogielski, Phys. Rev. Lett. **57**, 1251 (1986)
14. J. Bricmont, A. Kupiainen, Phys. Rev. Lett. **59**, 1829 (1987)
15. J.P. Sethna, K. Dahmen, S. Kartha, J.A. Krumhansl, B.W. Roberts, J.D. Shore, Phys. Rev. Lett. **70**, 3347 (1993); K. Dahmen, J.P. Sethna, Phys. Rev. Lett. **71**, 3222 (1993)
16. D.P. Belanger, A.R. King, V. Jaccarino, J.L. Cardy, Phys. Rev. B **28**, 2522 (1983)
17. P.-Z. Wong, J.W. Cable, Phys. Rev. B **28**, 5361 (1983)
18. R.J. Birgeneau, R.A. Cowley, G. Shirane, H. Yoshizawa, Phys. Rev. Lett. **54**, 2147 (1985)
19. T. Nattermann, J. Villain, Phase Transitions **11**, 5 (1988)
20. See, e.g. the articles by D. P. Belanger, T. Nattermann in *Spin Glasses and Random Fields*, edited by A.P. Young (World Scientific, Singapore, 1998)
21. R.J. Birgeneau, J. Magn. Magn. Mater. **177**, 1 (1998)
22. A.P. Young, M. Nauenberg, Phys. Rev. Lett. **54**, 2429 (1985)
23. M. Gofman, J. Adler, A. Aharony, A.B. Harris, M. Schwartz, Phys. Rev. Lett. **71**, 2841 (1993); M. Gofman, J. Adler, A. Aharony, A.B. Harris, M. Schwartz, Phys. Rev. B **53**, 6362 (1996)
24. M.S. Cao, J. Machta, Phys. Rev. B **48**, 3177 (1993)
25. M.E.J. Newman, B.W. Roberts, G.T. Barkema, J.P. Sethna, Phys. Rev. B **48**, 16533 (1993)
26. A. Falicov, A.N. Berker, S.R. McKay, Phys. Rev. B **51**, 8266 (1995)
27. M.R. Swift, A.J. Bray, A. Maritan, M. Cieplak, J.R. Banavar, Europhys. Lett. **38**, 273 (1997)
28. J.-C. Anglés d' Auriac, N. Sourlas, Europhys. Lett. **39**, 473 (1997)
29. N. Sourlas, Comput. Phys. Commun. **121**, 183 (1999)
30. A.K. Hartmann, U. Nowak, Eur. Phys. J. B **7**, 105 (1999)
31. J. Machta, M.E.J. Newman, L.B. Chayes, Phys. Rev. E **62**, 8782 (2000)
32. A.K. Hartmann, A.P. Young, Phys. Rev. B **64**, 214419 (2001)
33. A.A. Middleton, D.S. Fisher, Phys. Rev. B **65**, 134411 (2002)
34. M.E.J. Newman, G.T. Barkema, Phys. Rev. E **53**, 393 (1996)

35. M. Itakura, Phys. Rev. B **64**, 012415 (2001)
36. A. Malakis, N.G. Fytas, Eur. Phys. J. B **51**, 757 (2006)
37. A. Aharony, Phys. Rev. B **18**, 3318 (1978); A. Aharony, Phys. Rev. B **18**, 3328 (1978) (see also: T. Schneider, E. Pytte, Phys. Rev. B **15**, 1519 (1977); D. Andelman, Phys. Rev. B **27**, 3079 (1983))
38. A.B. Harris, J. Phys. C **7**, 1671 (1974)
39. A.N. Berker, Phys. Rev. B **29**, 5243 (1984); A.N. Berker, S.R. McKay, Phys. Rev. B **33**, 4712 (1986); A.N. Berker, Phys. Rev. B **42**, 8640 (1990); A.N. Berker, Physica A **194**, 72 (1993)
40. V.S. Dotsenko, J. Stat. Mech. (2007) P09005
41. J.T. Chayes, L. Chayes, D.S. Fisher, T. Spencer, Phys. Rev. Lett. **57**, 2999 (1986); R.R.P. Singh, M.E. Fisher, Phys. Rev. Lett. **60**, 548 (1988); F. Pázmándi, R.T. Scalettar, G.T. Zimányi, Phys. Rev. Lett. **79**, 5130 (1997); A. Aharony, A.B. Harris, S. Wiseman, Phys. Rev. Lett. **81**, 252 (1998)
42. M. Schwartz, M. Gofman, T. Nattermann, Physica A **178**, 6 (1991)
43. U. Nowak, K.D. Usadel, J. Esser, Physica A **250**, 1 (1998)
44. I. Dayan, M. Schwartz, A.P. Young, J. Phys. A **26**, 3093 (1993)
45. A. Aharony, A.B. Harris, Phys. Rev. Lett. **77**, 3700 (1996)
46. S. Wiseman, E. Domany, Phys. Rev. Lett. **81**, 22 (1998); S. Wiseman, E. Domany, Phys. Rev. E **58**, 2938 (1998)
47. G. Parisi, N. Sourlas, Phys. Rev. Lett. **89**, 257204 (2002)
48. A. Malakis, N.G. Fytas, Phys. Rev. E **73**, 016109 (2006)
49. N.G. Fytas, A. Malakis, Eur. Phys. J. B **50**, 39 (2006)
50. A. Efrat, M. Schwartz, e-print `arXiv:cond-mat/0608435`
51. L. Hernández, H. Ceva, e-print `arXiv:cond-mat/0702398; arXiv:cond-mat/07092159`
52. Y. Wu, J. Machta, Phys. Rev. Lett. **95**, 137208 (2005)
53. Y. Wu, J. Machta, Phys. Rev. B **74**, 064418 (2006)
54. A. Malakis, A. Peratzakis, N.G. Fytas, Phys. Rev. E **70**, 066128 (2004)
55. A. Malakis, S.S. Martinos, I.A. Hadjiagapiou, N.G. Fytas, P. Kalozoumis, Phys. Rev. E **72**, 066120 (2005)
56. L. Hernández, H.T. Diep, Phys. Rev. B **55**, 14080 (1997)
57. Vl.S. Dotsenko, W. Selke, A.L. Talapov, Physica A **170**, 278 (1991)
58. H. Rieger, A.P. Young, J. Phys. A **26**, 5279 (1993)
59. H. Rieger, Phys. Rev. B **52**, 6659 (1995)
60. W.C. Barber, D.P. Belanger, J. Magn. Magn. Mater. **226**, 545 (2001)
61. I. Dukovski, J. Machta, Phys. Rev. B **67**, 014413 (2003)
62. F. Wang, D.P. Landau, Phys. Rev. Lett. **86**, 2050 (2001); F. Wang, D.P. Landau, Phys. Rev. E **64**, 056101 (2001); D.P. Landau, F. Wang, Comput. Phys. Commun. **147**, 674 (2002); B.J. Schulz, K. Binder, M. Müller, D.P. Landau, Phys. Rev. E **67**, 067102 (2003)
63. C. Yamaguchi, Y. Okabe, J. Phys. A **34**, 8781 (2001); P.N. Vorontsov-Velyaminov, N.A. Volkov, A.A. Yurchenko, J. Phys. A **37**, 1573 (2004); M. Troyer, S. Wessel, F. Alet, Phys. Rev. Lett. **90**, 120201 (2003); N. Rathore, J.J. de Pablo, J. Chem. Phys. **116**, 7225 (2002); M.S. Shell, P.G. Debenedetti, A.Z. Panagiotopoulos, Phys. Rev. E **66**, 056703 (2002); P. Poulain, F. Calvo, R. Antoine, M. Broyer, Ph. Dugourd, Phys. Rev. E **73**, 056704 (2006); C. Zhou, T.C. Schulthess, S. Torbrügge, D.P. Landau, Phys. Rev. Lett. **96**, 120201 (2006)
64. Y. Okabe, Y. Tomita, C. Yamaguchi, Comput. Phys. Commun. **146**, 63 (2002)
65. Q. Yan, J.J. de Pablo, Phys. Rev. Lett. **90**, 035701 (2003)
66. N. Rathore, Q. Yan, J.J. de Pablo, J. Chem. Phys. **120**, 5781 (2004)
67. E.A. Mastny, J.J. de Pablo, J. Chem. Phys. **122**, 124109 (2005)
68. C. Zhou, R.N. Bhatt, Phys. Rev. E **72**, 025701(R) (2005)
69. A. Malakis, N.G. Fytas, Phys. Rev. E **73**, 056114 (2006)
70. S.S. Martinos, A. Malakis, I.A. Hadjiagapiou, Physica A **355**, 393 (2005)
71. A. Malakis, P. Kalozoumis, N. Tyraskis, Eur. Phys. J. B **50**, 63 (2006)
72. A. Malakis, P. Kalozoumis, N.G. Fytas, Rev. Adv. Mater. Sci. **14** 1 (2007)
73. A. Malakis, N.G. Fytas, P. Kalozoumis, Physica A **383**, 351 (2007)
74. I. Shteto, J. Linares, F. Varret, Phys. Rev. E **56**, 5128 (1997)
75. A.R. Lima, P.M.C. de Oliveira, T.J.P. Penna, Solid State Commun. **114**, 447 (2000)
76. C.J. Silva, A.A. Caparica, J.A. Plascak, Phys. Rev. E **73**, 036702 (2006)
77. S.-H. Tsai, F. Wang, D.P. Landau, Phys. Rev. E **75**, 061108 (2007)
78. M. Deserno, Phys. Rev. E **56**, 5204 (1997)
79. M. Blume, Phys. Rev. **141**, 517 (1966); H.W. Capel, Physica **32**, 966 (1966); H.W. Capel, Physica **33**, 295 (1967); H.W. Capel, Physica **37**, 423 (1967)
80. H.K. Lee, Y. Okabe, D.P. Landau, Comput. Phys. Commun. **175**, 36 (2006)
81. A.M. Ferrenberg, D.P. Landau, Phys. Rev. B **44**, 5081 (1991)
82. D. Andelman, A.N. Berker, Phys. Rev. B **29**, 2630 (1984); Y. Shapir, A. Aharony, J. Phys. C **14**, L905 (1984)
83. A.L. Talapov, H.W.J. Blote, J. Phys. A **29**, 5727 (1996)
84. L.W. Bernardi, S. Prakash, I.A. Campbell, Phys. Rev. Lett. **77**, 2798 (1996)
85. M.N. Barber, *Phase Transitions and Critical Phenomena*, edited by C. Domb, J.L. Lebowitz (Academic, NY, 1983)